# **Nanoscale**



PAPER View Article Online



Cite this: Nanoscale, 2017, 9, 1637

# Search for effective chemical quenching to arrest molecular assembly and directly monitor DNA nanostructure formation†

J. M. Majikes,\* J. A. Nash and T. H. LaBean

Structural DNA nanotechnology has demonstrated both versatility and potential as a molecular manufacturing tool; the formation and processing of DNA nanostructures has therefore been subject to much interest. Characterization of the formation process itself is vital to understanding the role of design in production yield. We present our search for a robust new technique, chemical quenching, to arrest molecular folding in DNA systems for subsequent characterization. Toward this end we will introduce two miniM13 origami designs based on a 2.4 kb scaffold, each with diametrically opposed scaffold routing strategies (maximized scaffold crossovers *versus* maximized staple crossovers) to examine the relevance of design in the folding process. By chemically rendering single strand DNA inert and unable to hybridize, we probe the folding pathway of several scaffolded DNA origami structures.

Received 27th October 2016, Accepted 25th December 2016 DOI: 10.1039/c6pr08433h

www.rsc.org/nanoscale

#### 1 Introduction

DNA nanotechnology<sup>1,2</sup> is a promising tool for challenges associated with nanoscale organization, ranging from creation of nanoscale actuators that target cancer cells<sup>3,4</sup> to controlled assembly of nanoelectronics.<sup>5,6</sup> Using DNA in a non-genetic, structural context raises many interesting processing and design questions, as doing so requires choosing the nucleobase sequences and complementary lengths of a large number of molecules in order to control their interactions. Understanding the design and processing of these supramolecular systems under diverse solution conditions has been a significant thrust of research. Examples range from increasing the efficiency of design cycles,<sup>7</sup> to predictive models for 3D structure,<sup>8-10</sup> to use of unorthodox buffers,<sup>11-13</sup> to assembly in deep eutectic solvents,<sup>14</sup> to conjugation and purification of nanostructures.<sup>15,16</sup>

Within design and processing, the formation of DNA nanostructures from single-strand DNA (ssDNA) to a predetermined double-strand DNA (dsDNA) structure is an interesting problem because the folding process directly links assembly

Department of Materials Science & Engineering, North Carolina State University, Raleigh, North Carolina 27606, USA. E-mail: jmmajike@ncsu.edu

† Electronic supplementary information (ESI) available: Initial tests for screening quencher candidates and determination of quencher excess (relative to nucleotide concentration). Code for circle map and base map generation is available online through nanohub (http://nanohub.org/tools/cadnanovis/). See DOI: 10.1039/c6nr08433h

yield to the design and choices that influence it. For scaffolded DNA origami, this process is akin to protein folding, as the viral scaffold is forced into its predetermined routing pattern by synthetic ssDNA, typically during thermal annealing. The design choices which influence DNA origami folding are myriad, ranging from the scaffold routing, the lattice choice, the use of half or full crossovers between neighbouring dsDNA helices, to modifying the number of bases between crossover connections which adds or removes overall stress and curvature.<sup>17</sup> A fuller understanding of design effects is increasingly valuable as new DNA nanostructures are created to address increasingly complex problems.

Many studies have addressed the folding process of scaffolded DNA origami. Folding yields have been studied in relation to staple break designs. 18 Exhaustive use of fluorophore quencher pairs has given insight into local binding rates.<sup>19</sup> Hot stage AFM has provided a useful window into the kinetics of DNA origami folding.20,21 Liquid nitrogen quenching has, through gel electrophoresis, monitored anneal progression.<sup>22</sup> Dimer scaffold molecules have been made to present each DNA molecule with a set of staple binding choices, through which folding preferences can be probed.<sup>23</sup> Notably, the surface binding of DNA nanostructures to mica recently has been used to quench and examine the folding process; this method has had significant success for 2D structures at a low concentration range.<sup>24</sup> In addition to experimental work, several theoretical models have been created to predict the folding processes of DNA nanostructures. 9,10 Despite the insights they provide, each of these techniques has Paper Nanoscale

drawbacks for systematic use. Conjugation of FRET pairs to DNA is expensive and requires purchasing a significant number of modified DNA strands for each new structure. The liquid nitrogen quench must be thawed before imaging, after which thermal motion will allow systems to continue developing, thus blurring the correspondence between temperature and folding state. Additionally, polymerization between structures could occur due to the large sections of scaffold left unsatisfied, requiring additional gel purification steps to remove. Examining nanostructure folding in situ requires both imaging under liquid, and temperature control, adding layers of difficulty, particularly for AFM where the surface binding interferes with and significantly alters the energetics of folding. Surface quenching of nanostructures requires large volumes at very low concentrations, which increases the cost of sampling, and limits the conditions under which systems can be quenched. Additionally, surface quenching is unlikely to work on 3D structure types. Together, these issues limit the conditions under which an arbitrary DNA self-assembly system may be examined. Each of these techniques produces interesting and useful information, but a more general tool to arrest and allow imaging of the folding process is highly desirable.

#### 1.1 Chemical quench

An alternative approach which could successfully avoid the drawbacks of other quenching strategies is to chemically alter a DNA system such that it is unable to continue folding. Such a system would render dsDNA unable to denature, or dehybridize, and render ssDNA unable to base pair, or hybridize, as shown in the top two panels of Fig. 1. The bottom left pane of

Fig. 1 illustrates chemical quenching of a structure containing both ssDNA and dsDNA. The bottom right illustrates the same structure treated with an imperfect quench which only prevents ssDNA from hybridizing *via* creation of adducts, but lacks crosslinking. A chemical quench would render DNA assembly unable to progress in either direction, and would be useful for any system whose progression is slower than the reactions associated with the quench.

In creating such a chemical quench, it is not necessary to develop new reagents. Numerous nucleic acid crosslinking protocols exist, such as those involving psoralen, nitrogen mustards, epichlorohydrin, and UV crosslinking. <sup>25–28</sup> Techniques which either render ssDNA inert, or permanently denature dsDNA, by creating chemical adducts are also common. <sup>29–32</sup> Despite the availability of such tools, development of an ideal chemical quench protocol presents several challenges; folding must be arrested while neither deforming nor excessively denaturing the dsDNA structure. For our search we only examined single reagents, rather than pairing reagents to create crosslinks and adducts separately. Towards this end, 8-methoxypsoralen, epichlorohydrin, glutaraldehyde, formaldehyde, and streptozotocin were screened, which is discussed in detail in the ESI.†

A major concern for a chemical quench is that the reagent rendering ssDNA inert will denature existing dsDNA, resulting in an imperfect quench shown in the bottom right of Fig. 1. Such a quencher, when added to a sample during thermal annealing to prevent further folding will partially denature that sample while rendering ssDNA inert. Due to this, the quenched samples will not perfectly represent the system at

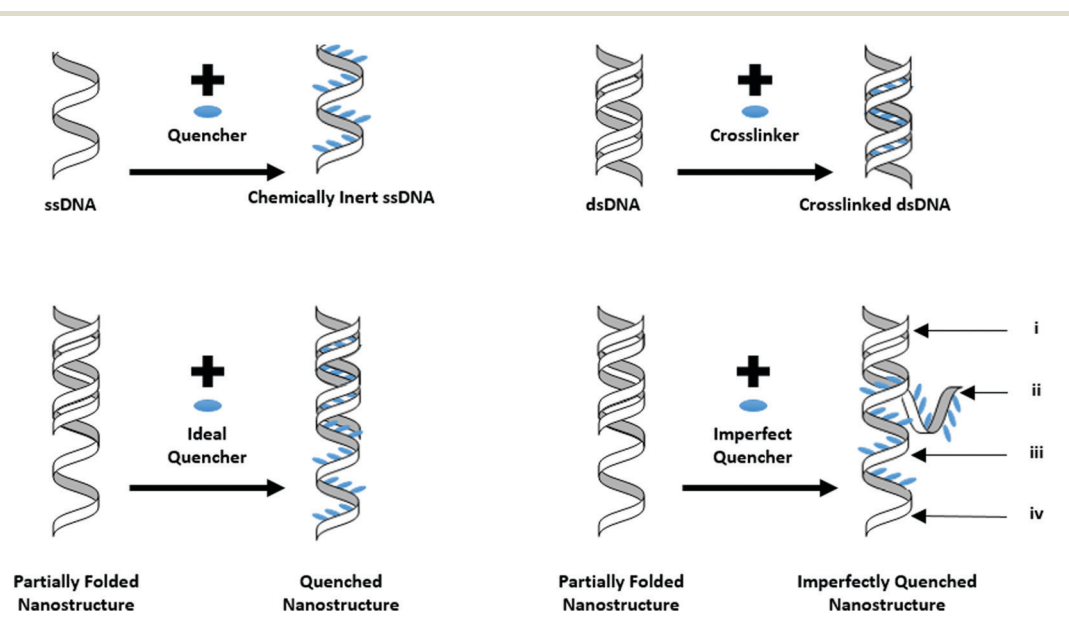


Fig. 1 Schematic of chemical quenching of DNA: top left – quenching of ssDNA, top right – quenching of dsDNA, bottom left – ideal quenching of a DNA nanostructure, bottom right – imperfect quenching of a DNA nanostructure in which crosslinking insufficiently occurs. i – dsDNA, ii – chemically denatured dsDNA, iii – inert ssDNA, iv – potentially unquenched ssDNA. Both ii and iv are characteristic of imperfect quenching, quencher excess and reaction time will determine whether ii or iv are present. It may not be possible to tune quencher concentration and quench time to ensure that neither ii nor iv are present.

Nanoscale

the temperature the quencher was added. However, such an imperfect quench will still accurately show the progression of the folding process. Creating a perfect quench using only a single reagent, rather than multiple quenching and crosslinking reagents, would require significant resources. As such, creating an imperfect quench is a first step, which may later be combined with a crosslinking step to develop a robust quenching protocol.

#### 1.2 DNA origami structures

Among DNA self-assembly strategies, DNA origami were chosen as the subject for chemical quenching as they form discrete objects where the unfolded scaffold may also be seen via AFM. Additionally, previous work on surface quenching was performed on an origami system,24 specifically the Rothemund Tall Rectangle, or TR.<sup>33</sup> As such, TR was chosen as the initial quench system, and two miniM13 scaffolded origami were designed, based loosely on the TR. The miniM13 scaffold is a 2.4 kb workbench scaffold, compared to the 7.2 kb wild type M13, and was chosen for the shorter design time and lower staple cost associated with the shorter scaffold.<sup>34</sup> As potential quenchers such as formaldehyde prefer to attack AT over GC nucleotides, 31 it is worth noting that the M13 origami have a 42% GC content while the miniM13 have a 49% GC content. These structures were created to examine the role of scaffold routing on folding by varying the distance between scaffold crossovers, changing the length of the scaffold "fingers". Reducing these finger lengths is one way to reduce the distance along the scaffold that the average staple must bridge; this should reduce the variance in conformational entropy penalties for the binding of various stable oligonucleotides.

Fig. 2 shows the three nanostructure test systems including the scaffold routing map, GC content map, and circle plot for each nanostructure. The circle plot illustrates the distance along the scaffold each crossover must bridge, as though it were the first to bind. The finger-112 structure, or F112, has the same width as the TR but one third the height due to the 2.4 kb length of the minM13 scaffold compared to the 7.2 kb wild type M13.34 The finger-16, or F16, structure has an identical footprint to the F112, which is to say it has the same dimensions and contact area with the substrate, but has greatly reduced finger size by forcing the scaffold to switch helices at each crossover. In this way the F112 architecture entails the minimum number of scaffold crossovers while F16 employs the maximum number of scaffold crossovers. When the edge staples on the left and right sides are left out, both the F112 and the F16 have identical numbers of total crossovers, including both scaffold and staples. Further crossover and staple motif information is discussed in the ESI.† Conformational entropy reduction of the scaffold has been identified as a major factor in the equilibrium folding of DNA origami. 23,24,35 The F112 and F16 were designed to examine whether structures with identical footprint, but different routing, would undergo significantly different folding processes.

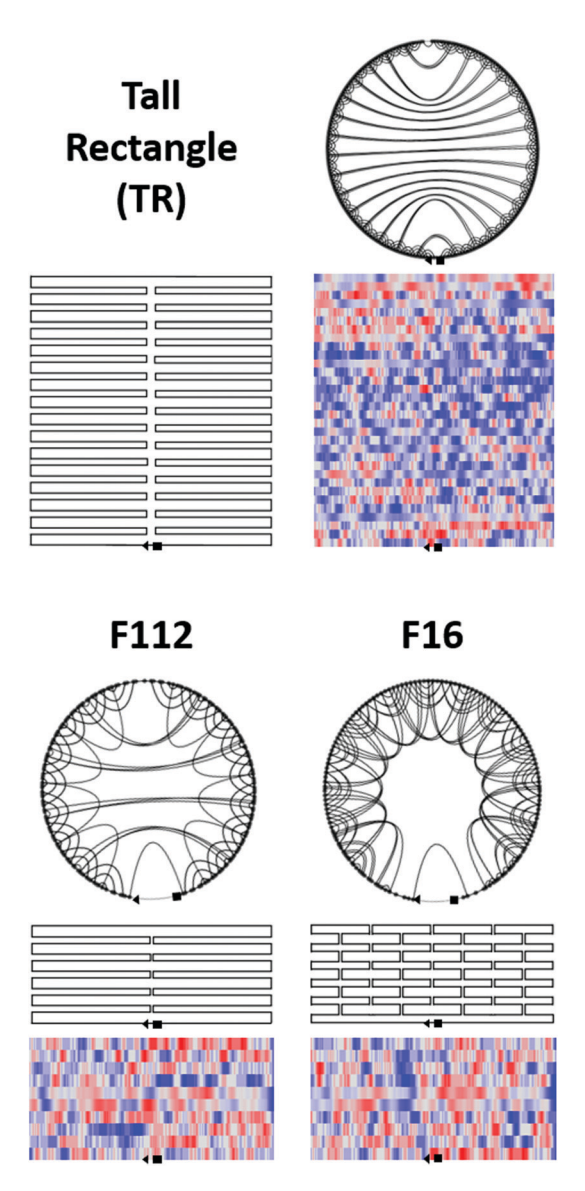
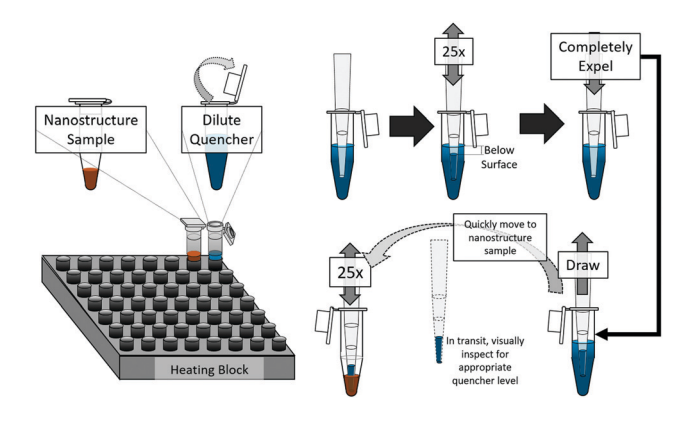


Fig. 2 Illustration of model DNA nanostructures. Top - Rothemund Tall Rectangle (TR), bottom left - finger 112 bases (F112), bottom right finger 16 bases (F16). Circle maps indicate bridging distance of staples for each structure. Routing maps show only the scaffold strand. GC content maps colored where red corresponds to high GC content and blue to low GC content.

## Experimental

All samples were annealed in sodium cacodylate buffer to avoid pH fluctuations with 12.5 mM Mg acetate at pH 5.5. Quenches were performed on 15 µL aliquots with 10× staples at 5 nM M13 scaffold, or 15 nM miniM13 scaffold. The miniM13 scaffold was used at increased concentration to ensure that the overall concentration of nucleotides was the same. Quenchers were added in excess, and were recorded relative to the total moles of nucleotides; for example, 500× formaldehyde refers to 500 times the number of moles of nucleotides in the aliquot to which formaldehyde is added.

Paper Nanoscale



**Fig. 3** Procedure for chemical quench inside a paused thermocycler. The quencher was pipetted up and down >25× to allow the pipette tip to thermally equilibrate. The quencher was then added to the nanostructure aliquot and pipetted up and down >25× to ensure mixing. The quencher aliquot was of large volume (100  $\mu$ L) to maintain constant temperature during pipette tip equilibration.

All quenchers were added to nanostructure aliquots in 7.5  $\mu$ L volumes. This experimental procedure is illustrated in Fig. 3. During chemical quenching the thermocycler was paused and the quencher was pipetted up and down 25 times to equilibrate the pipette tip to the quencher temperature. The quencher was then completely expelled and a fresh 7.5  $\mu$ L was drawn into the pipette tip, which was then quickly mixed into the sample aliquot, pipetting up and down 25 times. The sample was then allowed to incubate for 5 minutes before unpausing the thermocycler. Quenched samples continued to cool *via* the normal annealing schedule, from 80 °C to 25 °C over 2 hours. All AFM data was gathered on an Asylum Cypher model using biolever mini tips in 1× TAE Mg buffer supplemented with 5 mM NiCl<sub>2</sub>. All gels were 2% agarose run in 1× TAE Mg buffer.

Liquid nitrogen quenches were used as controls to determine initial quencher concentration and were performed using the protocol developed by Sobczak  $et~al.^{22}$  Fluorescence data were gathered in a QuantStudio 6 RT-PCR unit, at 5 nM scaffold 10× staples, annealing from 80–25 °C for 5.5 hours using Sybr green and Rox fluorescent dyes as reporter and reference respectively.

Circle maps were generated by drawing arcs, representing crossovers, along the outer circle, representing the scaffold. Web based tools to create circle plots from caDNAno .json files containing DNA origami designs are available from our nanohub tool (http://nanohub.org/tools/cadnanovis/).

## 3 Results and discussion

#### 3.1 Potential quenching agents

The initial potential quenching agents (8-methoxypsoralen, epichlorohydrin, glutaraldehyde, formaldehyde, and streptozotocin see ESI Fig. S1†) were evaluated, and formaldehyde was chosen. 8-Methoxypsoralen was rejected as its adducts did not prevent origami aliquots treated at 80 °C from folding (ESI

Fig. S2†). Streptozotocin was similarly ineffective (Fig. S3†), likely due to its degradation at high temperature. Initial tests indicated that epichlorohydrin, glutaraldehyde and formaldehyde are all able to arrest folding (Fig. S3 and S4†). Epichlorohydrin was set aside due to degradation concerns and as it requires solubilization in dimethyl sulfoxide, which presents additional safety concerns. Finally, formaldehyde was chosen over glutaraldehyde, as its interactions with nucleic acids are well documented, due to its use as a common fixitive. 29-31,36 The wealth of documentation on formaldehyde should help in creating effective protocols which address a broad range of concentrations, pHs, and temperatures. Although formaldehyde is known to be toxic, the FDA guidelines for its safe handling in concentrations >1%, or 0.1% in case of potential eye exposure are readily met by standard laboratory equipment and practices. 37,38 However, institutional guidelines for safe handling of formaldehyde may vary. To limit exposure with the ~1.2% formaldehyde, 100 µL stocks and the 0.8% formaldehyde, 27 µL samples, we used gloves, lab coats, and eye protection, and performed quenches in a fume hood. As AFM samples were diluted to 0.06% formaldehyde, only gloves were required for AFM sample preparation.

With both dsDNA and folded RNA, formaldehyde creates adducts, particularly on A and T bases, destabilizing double helical segments.<sup>31</sup> Because base stacking in helices interferes with the formation of adducts, the rate of dsDNA denaturation increases with helix breathing, or thermal fluctuations of the helix. As such, the reaction rate for ssDNA is much greater than for dsDNA.30,36 Additionally, strands closer to their melting temperature will be more rapidly denatured than helices far from their melting temperature due to increased thermal fluctuation. Over long periods at low temperature and low concentration, formaldehyde has been shown to crosslink dsDNA between exocyclic amines on AT/TA sequences. 39,40 At the temperatures and concentrations described here, formaldehyde readily arrested origami formation, but did not act as an effective crosslinker. The tendency of formaldehyde to more rapidly react with ssDNA, and dsDNA close to its melting temperature, is therefore fortunate. Formaldehyde alone is likely to act as an effective imperfect quencher.

Finally, it is worth noting that the formaldehyde adducts are reversible, a property that is used to recover nucleic acids from fixed tissues. Protocols to reverse formaldehyde adducts and crosslinks typically require incubation at 65–70 °C for several hours. <sup>29,41</sup> As such, de-quenching should not be a serious concern, particularly if the structures are stored at -20 °C or 4 °C as in this study.

#### 3.2 Initial formaldehyde quench

In order to establish experimental conditions, gel migration of a liquid nitrogen quench at 56 °C was compared to samples with various excesses of formaldehyde at the same temperature (ESI Fig. S3†). The closest match at 56 °C was quenched with 500× formaldehyde. This initial excess was used to quench TR across a wide temperature range in one degree increments. These samples were then compared by gel electro-

Nanoscale Paper

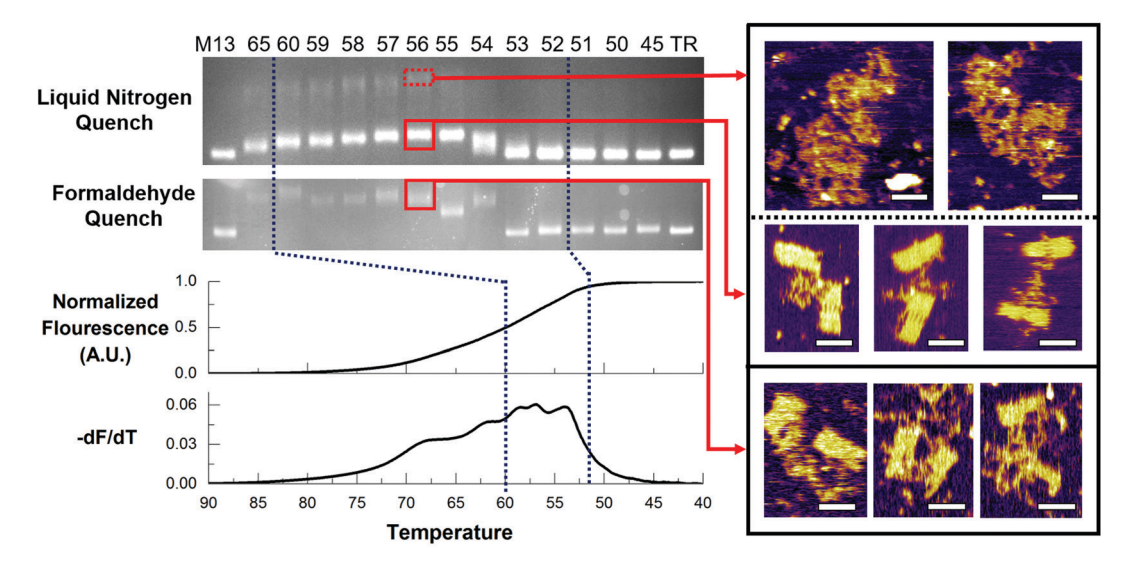


Fig. 4 Comparison of liquid nitrogen quench and formaldehyde quench (500x nucleotide concentration) of TR. Top - Agarose gel of liquid nitrogen quench over formaldehyde quench, bottom left - normalized fluorescence anneal curves with blue dotted lines to indicate corresponding temperature range. While the fluorescence anneal curves span the entire annealing process, the gel images address the ~50%-100% range of annealing, as this is likely to have the highest change in electrophoretic mobility. Right - AFM images of freeze 'N squeeze extraction from indicated bands. All scale bars are 50 nm.

phoresis to the liquid nitrogen quench and to the normalized fluorescence annealing curve of the same system.

Shown in Fig. 4 is the comparison of the chemical quench and liquid nitrogen quench and AFM images of the gel purified bands for 56 °C. The gels in Fig. 4 show a clear shift between 54-53 °C for both the liquid nitrogen and formaldehyde quenches which correspond to the plateau of the anneal curve. This shift likely corresponds to the fully formed TR being more compact than incompletely formed TR, whose ssDNA scaffold acts to reduce electrophoretic mobility. This shift also corresponds well to the fluorescence annealing data shown in Fig. 4 on the bottom left. The fluorescence data was normalized as per Sanford et al., such that zero indicates the system is entirely ssDNA and one indicates full formation. 42

The AFM images in Fig. 4 show reasonable agreement between the primary liquid nitrogen quench band and the formaldehyde quench, with some evident denaturing of the formaldehyde sample. The light secondary band in the liquid nitrogen quench, which is shown to be unfolded, is not present in the formaldehyde quench. This light band was present for similar nanostructures in previous work by Sobczak et al.<sup>22</sup>

Fig. 5 shows AFM images of formaldehyde quenches corresponding to the range of temperatures in Fig. 4, without gel purification. From Fig. 5, the formaldehyde quenches <56 °C depict a level of assembly one would anticipate from the anneal curve in Fig. 4. However, for formaldehyde quenches >56 °C, there is an increasing denaturation of the TR beyond what would be anticipated from fluorescence data; the curves in Fig. 4 would indicate 50% formation at 60 °C. Some of this apparent lack of folding could be due to independent binding of multiple copies of the same staple due to the staple excess.

As the formaldehyde excess for all temperatures shown was 500×, the increased denaturation of dsDNA is most likely due to the increased reaction rate of formaldehyde with increasing temperature. High structural fluctuation and increased helix breathing of the various dsDNA helices near their  $T_{\rm m}$  may also play a role.

Despite this denaturation, the folding pathway of the TR is clearly distinguishable. The loop of excess scaffold DNA visible in the 57 °C sample identifies that section of the nanostructure as the bottom of the TR. The small nodules visible on the scaffold at 57 °C indicate the staples which bridge the shortest distances along the scaffold are the first to fully bind. As the temperature decreases, the top section of the scaffold is drawn into shape, then the top and bottom slowly join with one another. These results match well with the recent surface quench of the TR structure performed by Wah et al.<sup>24</sup>

In both the chemical and surface based quench, it is clear that reductions in conformational entropy of the scaffold play an important role in the binding order of staples for the TR. The GC content map for the TR, shown in Fig. 2, also provides insight. Both the top and bottom of the TR have an increased GC content, but on the bottom, there is a line of high GC content which bridges the central seam. As the bottom half forms first, we can reasonably argue that the high GC content allows the reduction in conformational entropy associated with binding to occur at a higher temperature than the same section on the upper half. This is promising as it allows observation of the effect of known forces on the folding process.

Despite the success of the TR chemical quench, the increased denaturation with increasing temperature presents a problem for formaldehyde quenching, particularly for systems annealing at temperatures significantly different from the TR.

Paper Nanoscale

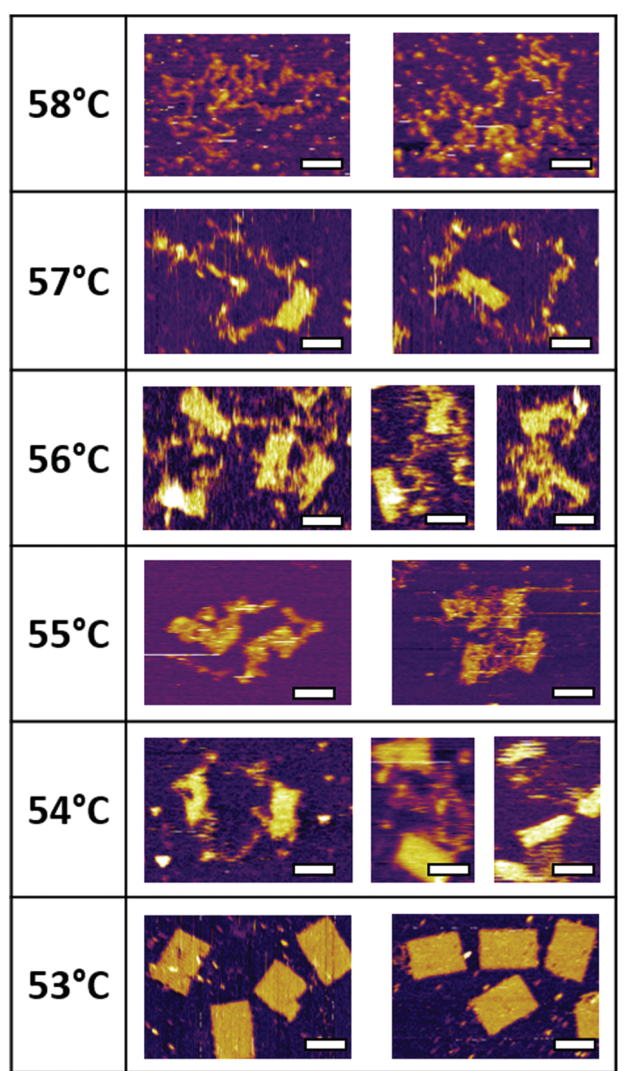


Fig. 5 AFM images of formaldehyde quenched TR (500x nucleotide concentration) with no additional gel purification as a function of quenching temperature. Scale bars 50 nm.

This concern comes into play for the F112 and F16, which anneal at a slightly higher temperature than the TR. For these structures at 15 nM, equivalent in nucleotide concentration to 5 nM TR, using 500× excess formaldehyde results in underquenching below 55 °C and nearly complete denaturation above 55 °C. Given this excessive denaturing it is possible that even if an additional crosslinker is added to quenching protocols, it could result in inaccurate quenching if the quencher excess is too high. At higher temperatures the formaldehyde could overwhelm a potential crosslinker while at much lower temperatures it might not be sufficient to prevent annealing.

#### 3.3 Formaldehyde excess and miniM13 structures (F112 & F16)

To address the poor results of using a static 500× excess for miniM13 structures, the minimal formaldehyde concentration to prevent annealing for a 5-minute incubation was found at several temperatures (ESI Fig. S6†). To provide an approximate

excess as a function of temperature for which the reaction proceeded to the same level of completion in the same time, these values were fitted to an exponential function, in anticipation of Arrhenius behaviour. Assuming a first order reaction rate, a linear relation can be used to find the desired excess of formaldehyde to reach the same degree of completion in five minutes for different concentrations (see discussion in the ESI†). This treatment neglects potential differences in rate constant with temperature, AT content, and proximity of dsDNA to its  $T_{\rm m}$ . The addition of crosslinking in a final protocol should prevent excess denaturing. The calculation for excess quencher is needed to ensure sufficient reaction with ssDNA, and to avoid an excess so high as to damage crosslinked dsDNA.

Quenches of the miniM13 F112 and F16 were performed at 5 nM miniM13, one third of the standard nucleotide concentration, using formaldehyde excesses calculated from eqn (S2) in the ESI.† Samples were performed in parallel starting with the F16, resulting in a longer incubation for F16 samples of approximately 30 seconds. The impacts of additional denaturation should therefore be stronger on the F16 structures. The F112 and F16 were quenched at 63 °C and 60 °C, since fluorescence annealing curves, obtained as for TR, indicated that the structures should be  $\sim$ 50–60% folded at those temperatures.

Fig. 6 shows AFM images of the F112 and F16 quenches, fully folded F112 and F16, and their respective fluorescence annealing curves (for melt curves and derivatives shown in ESI Fig. S7†). The partial folding shown in Fig. 6 indicate that adjusting the formaldehyde concentration for quenching temperature improved the imperfect formaldehyde quench from use of a static 500× formaldehyde.

Given the limitations of the imperfect formaldehyde quench, these quenches were imaged to show both the breadth of transition, and to compare the F112 and F16 rather than to determine their entire folding pathway. As conformational entropy penalties are important in scaffold folding, the F16 (short loops) was designed to form at a higher temperature than the F112 (long loops). The annealing curves in Fig. 6 show that while the F16 appears to be more completely annealed at all temperatures than the F112, the difference is not as dramatic as one might have anticipated based on differences in the circle plots in Fig. 2. The circle plots provide a useful snapshot which indicates conformational entropy penalties, but cannot be used to estimate  $T_{\rm m}$ . Additionally, the best ways to interpret the distribution of penalties indicated by the circle plots are not yet fully understood (design information of F112/F16 shown in ESI Fig. S8†).

Given the similar fluorescence anneal curves of the F112 and F16 in Fig. 6, it is not surprising that AFM imaging indicates that the F16 and F112 structures are formed to a similar degree; further development and implementation of quantitative image analysis could allow evaluation of precise fractions of formation which could be compared to anneal curves. While the 63 °C and 60 °C F112 images are reminiscent of the TR at 57 °C and 56 °C, the partially formed F16 quenched at 63 °C is more irregular as though folding from multiple

Nanoscale Paper

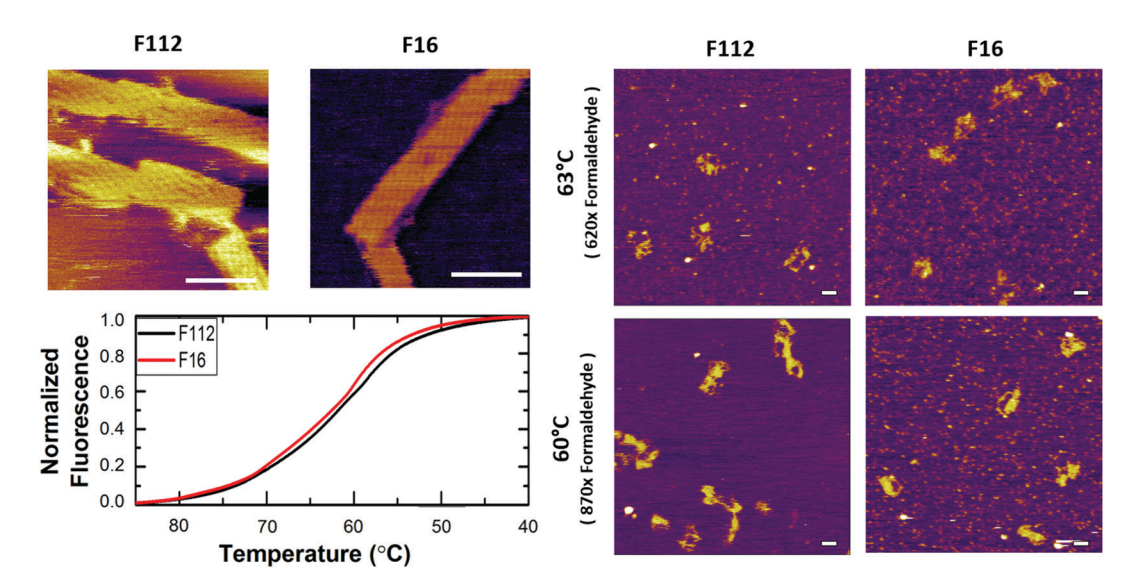


Fig. 6 AFM images of formaldehyde quenched F16 and F112 at 63 C (top right) and 60 C (bottom right). Top left shows - AFM images of fully formed F112 and F16, bottom left - normalized fluorescence anneal curves and fully annealed origami. (620x and 870x formaldehyde respectively) Scale bars 50 nm.

initiation points. This is reasonable as the F16 has significantly different symmetry and more stable binding locations with approximately equal conformational entropy penalties.

While the data in Fig. 6 are promising, more detailed examination of folding pathways would be best performed with a complete quench including a crosslinker along with the adduct creating formaldehyde. Such a procedure would provide two benefits. The first is the ability to directly relate substructure folding with fluorescence annealing data; an imperfect quench cannot provide such information. This will better characterize the link between design and folding properties. The second benefit is that it should reduce human sampling and timing errors. As the formaldehyde denatures folded dsDNA, an imperfect quench is quite sensitive to temperature fluctuations and the time an aliquot is incubated before continuing the thermal anneal. Inclusion of a crosslinking agent should significantly improve consistency of the quenches.

## Conclusions

In conclusion, we have demonstrated that a partial chemical quench consisting of only formaldehyde can be used to probe the folding process of DNA based nanostructures. Our results show reasonable agreement with the literature for Tall Rectangle origami folding.24 Additionally, we are able to show that scaffold routing plays a role in folding for identically shaped origami as evidenced through the F16 and F112 nanostructures.

We expect that integration of an additional crosslinking step to the chemical quench strategy should result in protocols which enable easy inspection of arbitrary DNA nanostructures, at arbitrary concentration, at any point in the folding process. Such capabilities would significantly improve current tools to

characterize folding. We consider crosslinkers such as 8-methoxypsoralen or epichlorohydrin to be promising in this regard, although nitrogen mustards have also been used to crosslink DNA nanostructures, a suitable candidate which does not degrade at higher temperatures would need to be found. 25,26,28 Overall, this study shows a proof of concept for, and the potential value of, a chemical quench protocol for DNA nanotechnology. Chemical quenching has potential benefits over other recent techniques as it does not require additional gel purification (liquid nitrogen quench) and has the ability to examine 3D structures (surface quench).

## Acknowledgements

The authors acknowledge funding from the US National Science Foundation to THL (NSF-ECCS-EPMD-1231888) and through a Graduate Research Fellowship (DGE-0946818) to JAN.

The authors acknowledge the Lommel lab at NC State University for providing access to Quantstudio 6 RT-PCR equipment and Dr Tim Sit for technical advice and training.

### Notes and references

- 1 N. C. Seeman, Structural DNA Nanotechnology, 2016.
- 2 H. Li, J. D. Carter and T. H. LaBean, Mater. Today, 2009, 12, 24-32.
- 3 Y.-X. Zhao, A. Shaw, X. Zeng, E. Benson, A. M. Nyström and B. Högberg, ACS Nano, 2012, 6, 8684-8691.
- 4 S. M. Douglas, I. Bachelet and G. M. Church, Science, 2012, 335, 831-834.
- 5 R. Campos, S. Zhang, J. M. Majikes, L. C. C. Ferraz and T. H. LaBean, Chem. Commun., 2015, 51, 14111-14114.

**Paper** 

- 6 E. C. Samano, M. Pilo-Pais, S. Goldberg, B. N. Vogen, G. Finkelstein and T. H. LaBean, Soft Matter, 2011, 7, 3240-
- 7 S. M. Douglas, A. H. Marblestone, S. Teerapittayanon, A. Vazquez, G. M. Church and W. M. Shih, Nucleic Acids Res., 2009, 37, 5001-5006.
- 8 D. Kim, F. Kilchherr, H. Dietz and M. Bathe, Nucleic Acids Res., 2011, 1, 1-7.
- 9 F. Dannenberg, K. E. Dunn, J. Bath, A. J. Turberfield and T. E. Ouldridge, J. Chem. Phys., 2015, 143, 165102.
- 10 J. M. Arbona, J. Elezgaray and J. P. Aimé, EPL, 2012, 100, 28006.
- 11 T. G. Martin and H. Dietz, Nat. Commun., 2012, 3, 1103.
- 12 J. Lee, R. Amin, B. Kim, S. J. Ahn, K. W. Lee, H. J. Kim and S. H. Park, Soft Matter, 2012, 8, 619.
- 13 H. Kim, S. P. Surwade, A. Powell, C. O. Donnell and H. Liu, Chem. Mater., 2014, 26, 5265-5273.
- 14 I. Gállego, M. A. Grover and N. V. Hud, Angew. Chem., Int. Ed., 2015, 54, 6765-6769.
- 15 A. Shaw, E. Benson and B. Hogberg, ACS Nano, 2015, 9, 4968-4975.
- 16 G. Bellot, M. A. McClintock, C. Lin and W. M. Shih, Nat. Methods, 2011, 8, 192-194.
- 17 C. E. Castro, F. Kilchherr, D. Kim, E. L. Shiao, T. Wauer, P. Wortmann, M. Bathe and H. Dietz, Nat. Methods, 2011,
- 18 Y. Ke, G. Bellot, N. V. Voigt, E. Fradkov and W. M. Shih, Chem. Sci., 2012, 3, 2587.
- 19 X. Wei, J. Nangreave, S. Jiang, H. Yan and Y. Liu, J. Am. Chem. Soc., 2013, 135, 6165-6176.
- 20 J. Song, Z. Zhang, S. Zhang, L. Liu, Q. Li, E. Xie, K. V. Gothelf, F. Besenbacher and M. Dong, Small, 2013, 9, 2954-2959
- 21 J. Song, J.-M. Arbona, Z. Zhang, L. Liu, E. Xie, J. Elezgaray, J.-P. Aime, K. V. Gothelf, F. Besenbacher and M. Dong, J. Am. Chem. Soc., 2012, 134, 9844-9847.
- 22 J.-P. J. Sobczak, T. G. Martin, T. Gerling and H. Dietz, Science, 2012, 338, 1458-1461.

- 23 K. E. Dunn, F. Dannenberg, T. E. Ouldridge, M. Kwiatkowska, A. J. Turberfield and J. Bath, Nature, 2015, 82-86.
- 24 J. L. T. Wah, C. David, S. Rudiuk, D. Baigl and A. Estevez-Torres, ACS Nano, 2016, 10, 1978-1987.
- 25 A. Rajendran, M. Endo, Y. Katsuda, K. Hidaka and H. Sugiyama, J. Am. Chem. Soc., 2011, 133, 14488-14491.
- 26 K. P. Romano, A. G. Newman, R. W. Zahran and J. T. Millard, Chem. Res. Toxicol., 2007, 20, 832-838.
- 27 M. Tagawa, K. Shohda, K. Fugimoto and A. Suyama, Soft Matter, 2011, 7, 10931-10934.
- 28 D. Zhang and P. J. Paukstelis, ChemBioChem, 2016, 1163-1170.
- 29 J. D. Mcghee and P. H. von Hippel, Biochemistry, 1975, 14, 1297-1303.
- 30 J. D. McGhe and P. H. von Hippel, Biochemistry, 1977, 16, 3267-3276.
- 31 J. D. McGhee and P. H. von Hippel, Biochemistry, 1975, 14, 1281-1296.
- 32 R. Jungmann, T. Liedl, T. L. Sobey, W. Shih and F. C. Simmel, J. Am. Chem. Soc., 2008, 130, 10062-10063.
- 33 P. W. K. Rothemund, Nature, 2006, 440, 297-302.
- 34 S. Brown, J. Majikes, H. Fennell, E. C. Samano and T. H. LaBean, Nanoscale, 2015, 4434, 16621-16624.
- 35 J.-M. Arbona, J.-P. Aimé and J. Elezgaray, J. Chem. Phys., 2013, 138, 15105.
- 36 J. D. McGhee and P. H. von Hippel, Biochemistry, 1977, 16,
- 37 Occupations safety and health standards, Code of Federal Regulations 29 CFR 1910.1048, (2016).
- 38 Formaldehyde: Food additive Listing, Code of Federal Regulations, 21 CFR 573.460, 2016.
- 39 H. Huang and P. B. Hopkins, J. Am. Chem. Soc., 1993, 115, 9402-9408.
- 40 M. Kawanishi, T. Matsuda and T. Yagi, Front. Environ. Sci., 2014, 2, 1-8.
- 41 S. Niranjanakumari, E. Lasda and R. Brazas, Methods, 2002, 26, 182-190.
- 42 L. N. Sanford, J. O. Kent and C. T. Wittwer, Anal. Chem., 2013, 9907-9915.